CARBON letters

Original Articles
Carbon Letters Vol. 27, 18-25 (2018)

Graphene nanosheets encapsulated poorly soluble drugs with an enhanced dissolution rate

Shou-Cang Shen[1,♠], Wai Kiong Ng[1], Kumaran Letchmanan[1], Ron Tau Yee Lim[1] and Reginald Beng Hee Tan[1,2,♠]

[1]Institute of Chemical and Engineering Sciences, A*STAR (Agency for Science, Technology and Research), Singapore 627833
[2]Department of Chemical and Biomolecular Engineering, The National University of Singapore, Singapore 117576

Article Info
Received 6 December 2017
Accepted 4 January 2018

♠Corresponding Author
E-mail: reginald_tan@ices.a-star.edu.sg
E-mail: shen_shoucang@ices.a-star.edu.sg
Tel: +65-6796-3841

Open Access
DOI: http://dx.doi.org/10.5714/CL.2018.27.018

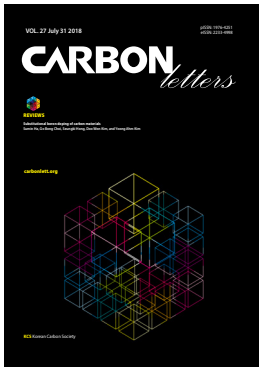

http://carbonlett.org

pISSN: 1976-4251
eISSN: 2233-4998

Abstract

In this study, graphene oxide(GO) was used as drug carriers to amorphize poorly water-soluble drugs via a co-spray drying process. Two poorly water-soluble drugs, fenofibrate and ibuprofen, were investigated. It was found that the drug molecules could be in the graphene nanosheets in amorphous or nano crystalline forms and thus have a significantly enhanced dissolution rate compared with the counterpart crystalline form. In addition, the dissolution of the amorphous drug enwrapped with the graphene oxide was higher than that of the amorphous drug in activated carbon (AC) even though the AC possessed a larger specific surface area than that of the graphene oxide. The amorphous formulations also remained stable under accelerated storage conditions (40°C and 75% relative humidity) for a study period of 14 months. Therefore, graphene oxide could be a potential drug carrier and amorphization agent for poorly water-soluble drugs to enhance their bioavailability.

Key words: graphene oxide, capsulation, dissolution rate, crystallinity, physical stability

1. Introduction

In recent years, a new nanostructured graphene with a two-dimensional carbon sheet form has led to new opportunities in electronics, sensors, and energy industrial sectors [1,2]. Graphene oxide is an oxidative derivative of graphene with additional functional groups, such as carboxyl, hydroxyl, carbonyl, and epoxide, on the surface of each sheet [3,4]. The presence of these functional groups has enabled graphene oxide to interact with its targeted molecules via various mechanisms such as physical adsorption, hydrogen bonding or covalent binding. Moreover, nanostructured graphene oxide also provides a wide platform for applications in biomedical areas [5]. Graphene has been widely investigated as drug carriers for effective drug delivery [6-8], and it has been reported that composites of graphene and polymers have enabled excellent controlled release of drugs [9-11]. The reduced form of graphene oxide [12] or graphene oxide functionalized with starch was shown to have pH-responsive drug delivery properties. It has been reported that graphene oxide nano-vehicles were used for targeted delivery of anticancer drugs with a good controlled drug release efficiency [13-15]. Moreover, graphene oxide has been developed together with a ferrite composite to control drug delivery and enable multifunctional magnetic resonance imaging [16-18]. Toxicity testing has indicated that prepared nanostructured graphene oxide has negligible hemolytic activity, which demonstrates its safety in a drug delivery system [6]. Although an animal in vivo test showed that the existence of graphene in the lungs via instillation administration might cause an inflammation response [19-21] graphene oxide and its derivatives were found to have very limited intestinal adsorption and were rapidly excreted in adult mice when orally administered [22,23]. The low absorption and cytotoxicity in the digestive system imply that graphene oxide could be potentially used for oral drug delivery.

Among the techniques for drug delivery, the delivery of poorly water-soluble drugs remains a

major challenge for new drug development because a large number of drug candidates and new chemical entities have low solubility and a low dissolution rate. Because of their low bioavailability, the commercialization of these drugs or new chemical entities remains challenging and difficult. For some marketed products, the low efficacy is attributed to the low solubility of the active pharmaceutical ingredients (APIs), and subsequently, a higher dosage is required to achieve the targeted therapeutic concentration which is not desirable due to side effects and patient compliance. Tremendous efforts/approaches have been made to enhance the dissolution and solubility of poor water soluble APIs. Among these processes, formulating poorly soluble APIs in amorphous form is an effective approach. Generally, the amorphous form has a much higher dissolution rate and apparent solubility compared to its crystalline form. Recently, mesoporous silica and carbon materials have been extensively investigated for the formulation of poorly water-soluble drugs in amorphous form or nano-crystalline form due to their nano-space confinement of the APIs [24-28]. Nevertheless, development is still on going for clinical applications using mesoporous materials in innovative formulations of poorly water-soluble drugs. Alternatively, graphene oxide is another potential platform that could be used for the delivery of poorly water-soluble drugs.

In this study, multilayer graphene oxide was used as a drug carrier for the formulation of poorly water-soluble APIs by co-spray drying a suspension of the graphene and API solution in ethanol. The resulting solid dispersion showed a significant enhancement in the dissolution rate profiles of poorly soluble drugs, such as IBU and FEN. Although graphene is a non-porous material, the API enwrapped in the nanosheets was in amorphous form and showed excellent stability during the storage test. To the best of our knowledge, the use of nanostructured graphene oxide as a drug carrier in the formulation of poorly soluble drugs to the enhance dissolution has rarely been reported before.

2. Experimental

2.1. Co-spray drying

Typically, to load 25 wt% fenofibrate (FEN; Sigma-Aldrich, USA) with graphene oxide (Sigma-Aldrich), 0.25 g of FEN was dissolved in 100 mL of ethanol (Fisher Scientific Ltd, UK), and 0.75 g of graphene oxide (Sigma-Aldrich, USA) were dispersed in the solution under stirring condition overnight. The spray drying was performed using a BÜCHI B-290 mini spray dryer (BÜCHI Labortechnik AG, Flawil, Switzerland) operated in the inert loop mode with N_2 flow. The inlet temperature was set to 81°C, and the resulting outlet temperature was approximately 50–55°C. The feed rate was 4.0 mL min^{-1}. The designed drug loading could be varied by changing the amount of FEN and graphene oxide in the mixture suspension. A similar preparation procedure and co-spray drying condition were performed using another poorly water-soluble drug ibuprofen (IBU; Sigma-Aldrich).

2.2. Powder X-ray diffraction (XRD)

Powder X-ray diffraction was performed using a D8-ADVANCE (Bruker) X-ray diffractometer in steps of 0.02° using Cu Kα radiation as the X-ray source. The measurement conditions were as follows: target, Cu; filter, Ni; voltage, 40 kV; current, 10 mA; scanning speed, 2°/min.

2.3. Scanning electron microscopy (SEM)

The particle morphology was examined by high resolution scanning field emission electron microscopy (SEM, JSM-6700F, JEOL, Japan). The spray dried pure FEN was coated with gold using a sputter coater (Cressington Sputter Coater 208HR, UK) for 1 min. Graphene oxide is a conductive material, and it was not necessary to coat the formulated sample with gold prior to the measurement as conventional organic API particles.

2.4. Differential scanning calorimetry and thermogravimetric analysis

Differential scanning calorimetry (DSC) was performed using a SDT 2960 simultaneous TGA-DSC thermogravimetric analyzer (TA Instrument Co., USA). Ten milligrams of sample were used in each experiment. The sample was heated from room temperature to 150°C under a nitrogen flow of 100 mL min^{-1} with a heating rate of 10°C/min.

2.5. N_2 adsorption

Nitrogen adsorption/desorption isotherms were measured using an Autosorb-6B gas adsorption analyzer (Quantachrome) at a temperature of –196°C. Before the nitrogen adsorption-desorption measurements, each sample was degassed at 40°C under a vacuum for 24 h. The specific surface area of the samples was determined from the linear portion of the Brunauer-Emmett-Teller plots.

2.6. Water vapor dynamic adsorption and desorption

Sorption isotherms of samples were obtained using dynamic vapor sorption (DVS Advantage, Surface Measurement Systems, Alperton, UK). The humidity range was varied from 0 relative humidity (RH) to 90% RH in steps of 10% RH at 40°C. The instrument was run in the dm/dt mode to decide when equilibrium had been reached with a reported 33 dm/dt set at 0.002% RH/min within an interval of 5 min. Approximately 10–12 mg of sample were used for each run.

2.7. In vitro drug release studies

Prior to the dissolution test, 25 mg of IBU or equivalent to 25 mg of IBU in an IBU/GO solid dispersion were pressed into a tablet with 800 mg of cornstarch. Dissolution of the IBU loaded samples was performed using 900 mL of 0.1N HCl solution at 37°C in the USP dissolution apparatus II (VK7010 dissolution tester, Varian Co, UK). The stirring speed was set to 100 rpm and about 5 mL medium samples were withdrawn manually for analysis at the specified time-points (5, 10, 15, 20, 30, 60, and 120 min) during the 2 h dissolution. The sample was filtered with a 0.20 μm nylon filter prior to the UV analysis at 220 nm using a UV spectrophotometer (Cary 50 spectrophotometer,

Varian). The dissolution medium for FEN was 0.1 N HCl in the presence of 0.5% Tween-80 surfactant, and the UV analysis was performed at 286 nm. FEN or FEN/GO was pressed into a tablet with 800 mg of cornstarch, and each tablet had 20 mg of FEN. The dissolution experiment was done in triplicate.

3. Results and Discussion

Fig. 1 shows the SEM images of graphene oxide and FEN loaded on graphene oxide with different loadings as well as the spray dried pure FEN. The graphene oxide had a morphology of "crumpled sheets" with the particle size ranging from submicron to several microns. The morphology of the graphene oxide was not significantly changed after being loaded with 25 wt% FEN by the co-spray drying process. Most of the FEN particles were enwrapped within the "crumpled graphene sheets." When the drug loading was increased to 50 wt%, part of the FEN was observed on the external surface of the graphene oxide with the primary particles and served as a binder to form agglomerations. Nevertheless, the particle size was still much smaller than that of the spray dried pure FEN, which showed a larger needle-like morphology with the particle size at several tens of microns. The presence of graphene oxide particles in the liquid suspension is believed to break the spray dried drops to a smaller size during the spray drying process, and thus, much smaller solid dispersion particles were obtained.

Fig. 2 shows the DSC curves of the FEN/GO formulations with different drug loadings. The endothermic peak at a temperature range of 76−100°C for the pure FEN was attributed to the melting of the crystalline FEN. When FEN was co-spray dried with graphene at a ratio of 50:50 (wt.), the corresponding endothermic peak was significantly reduced and shifted to a lower temperature range of 72–82 °C. The result implies that the crystallinity of the loaded FEN was decreased after the co-spray drying process, and the particle size reduction of the FEN on the graphene oxide may result in a lower melting temperature [29]. When the drug loading was reduced to 35 wt%, the endothermic peak was further reduced. It was noted that the endothermic peak completely disappeared when 25 wt% of FEN was loaded onto graphene oxide, indicating that FEN was in the amorphous form at this drug loading. The physical transformation of the crystallinity of FEN via co-spray drying with graphene oxide was also revealed by the XRD measurement shown in Fig. 3. The XRD pattern of the 25 wt% FEN loaded on the graphene oxide was identical to the pure graphene oxide, and no characteristic peaks for FEN crystal from the loaded FEN with graphene could be detected by X-ray diffraction indicating that FEN/GO (25 wt%) was in an X-ray amorphous form. For the samples of graphene oxide loaded with 35 or 50 wt% FEN, the diffraction characteristic peaks attributed to the FEN crystal could be observed but at a much lower intensity compared to the untreated raw FEN crystal. As shown in Fig. 4, the morphology and physical state of FEN/GO were also investigated by

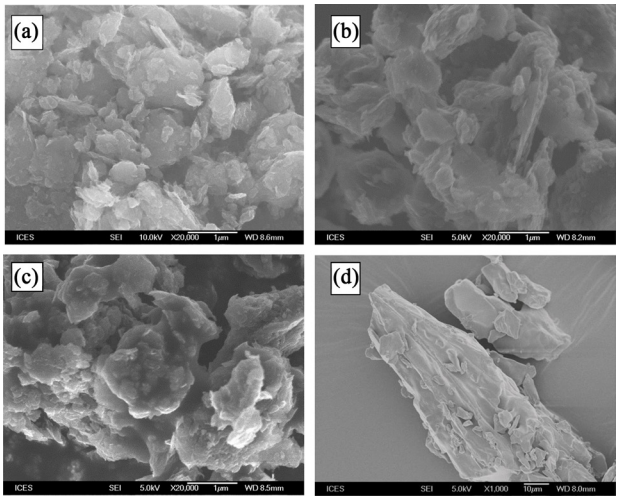

Fig. 1. (a) GO, (b) FEN2 5%/GO and (c) FEN 50%/GO, (d) spray dried FEN.

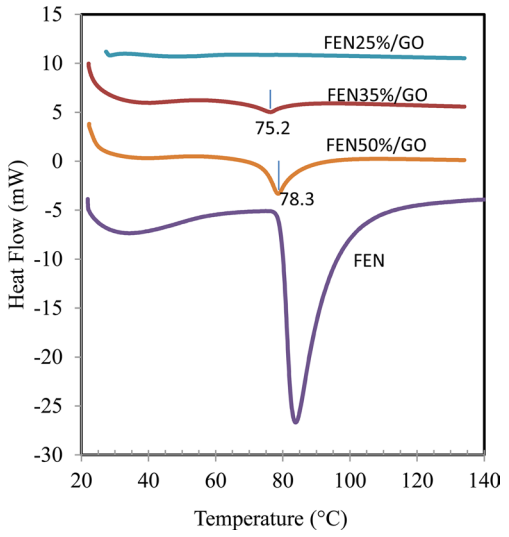

Fig. 2. DSC curves of the FEN co-spray dried with graphene oxide with different drug loadings.

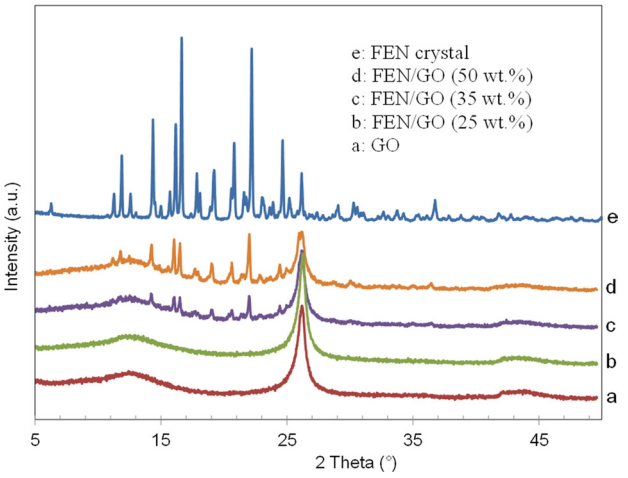

Fig. 3. XRD patterns of the FEN co-spray dried with graphene oxide at different loadings and compared with the pure FEN as well as graphene oxide.

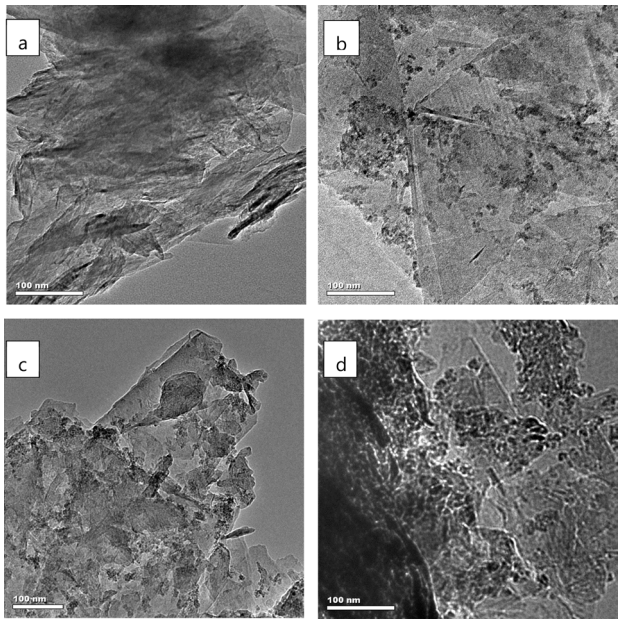

Fig. 4. TEM images of (a) GO and GO loaded FEN with loadings of (b) 25 wt%, (c) 35 wt% and (d) 50 wt%.

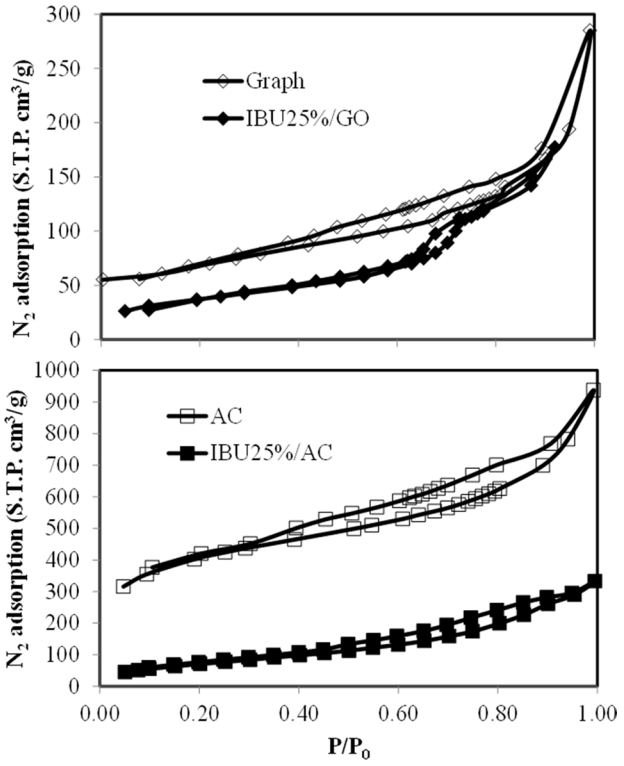

Fig. 5. N_2 adsorption-desorption isotherms of the 25% IBU loaded on graphene oxide and AC compared with the pure drug carriers.

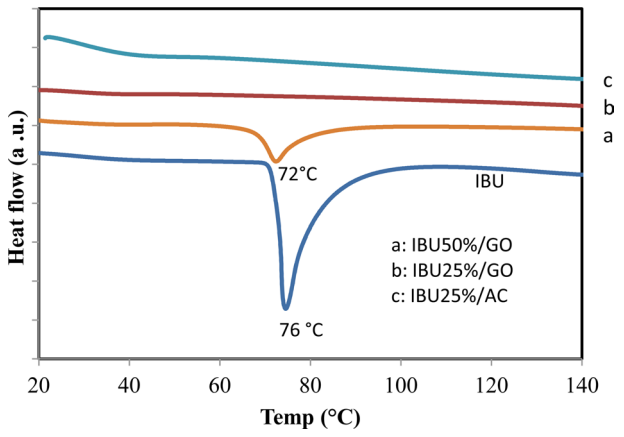

Fig. 6. DSC curves of the IBU co-spray dried with graphene oxide and activated carbon.

TEM measurement. The pure graphene oxide showed randomly stacked nano-sheet structures. There were nanoscale-sized interstices among the crumpled sheet structures. After co-spray drying with FEN, the small solution drops in the interstices would rapidly dry to form nanoparticles on the surface of the graphene oxide. As seen in Fig. 4b, when the drug loading was 25 wt%, small particles at several nano meters could be observed on the graphene oxide, and the particles were evenly distributed. The graphene oxide with its nanostructure well separated the small particles at the different interstices and prevented the growth of FEN nuclei to form crystal structures. Thus, the loaded FEN was in amorphous form. When the drug loading was increased to 35 wt%, some FEN particles may stay on the external surface of the graphene oxide particles and form crystals in addition to the amorphous small particles in the interstices among the graphene sheets. With the increment of the drug loading, more FEN particles on the external surface could be observed (Fig. 4d), and they formed crystal agglomerates which was in agreement with the higher crystallinity detected by XRD and DSC.

Poorly water-soluble IBU was also co-spray dried with graphene oxide and compared with conventional highly porous activated carbon with a large surface area. The results of the N_2 adsorption measurement indicated that the activated carbon had a large specific area of 1364.1 $m^2 g^{-1}$, whereas the graphene oxide had a specific surface area of 236.5 $m^2 g^{-1}$. After loading with 25 wt% IBU by the co-spray drying process, the surface area of the activated carbon loaded with IBU was significantly reduced by 80% to 271.1 $m^2 g^{-1}$. As for the graphene oxide loaded with IBU, it only showed a 43% reduction in the specific surface area (135.7 $m^2 g^{-1}$). As seen in Fig. 5, the amount of N_2 adsorption on the activated carbon was significantly decreased after loading with IBU at all the relative pressure ranges. In comparison, the amount of N_2 adsorption on the graphene oxide was not substantially reduced, especially at a high P/P_0 range above 0.75. Activated carbon is a highly porous carbon material, for which the internal surface of the pore walls contributes to the majority of its specific surface area. Upon co-spray drying the suspension of activated carbon and IBU, most of the IBU molecules were loaded into the pore structures by rapid capillary condensation, thus causing a significant reduction in the pore volume and specific surface area of the activated carbon. Figure 6 shows the DSC curves of the IBU co-spray dried with the graphene

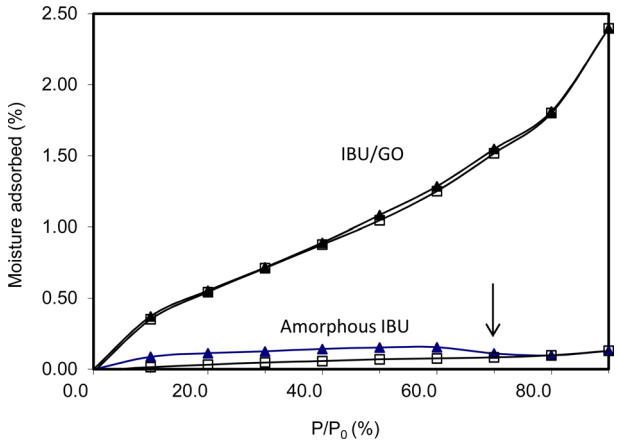

Fig. 7. DVS curves of the IBU loaded on graphene oxide and compared with the pure amorphous IBU (solid: adsorption, empty: desorption).

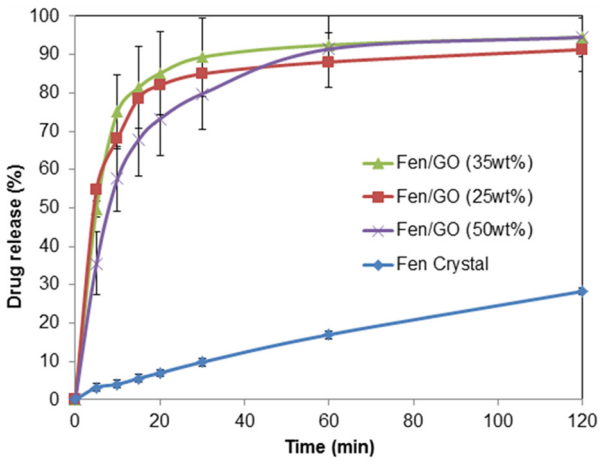

Fig. 8. Dissolution profiles of the FEN/GO with different loadings and compared with the untreated FEN crystal.

oxides and activated carbon. The untreated IBU crystal showed an endothermic peak at 76°C, attributed to the melting point of IBU. For the 50 wt% IBU loaded on graphene oxide sample, the endothermic peak was significantly reduced and shifted to 72°C. This endothermic peak was not observed for the 25wt% IBU loaded on either the graphene oxide or activated carbon, implying both samples were in amorphous form. For activated carbon, the microporous structures with a large surface area confined the particles of IBU and prevented their re-crystallization. The GO with its nanostructure is believed to encapsulate the IBU and avoid the formation of nuclei for crystal growth during the rapid drying process. Because the specific surface area of the graphene was not as large as AC or mesoporous silica, the loading of the amorphous form of IBU and FEN on non-porous graphene oxide was limited to 25 wt%. Higher loadings of APIs might cause the re-crystallization of the APIs on the surface of the graphene oxide because graphene oxide nanosheets do not possess a large pore volume to confine the APIs in amorphous form. Partial API molecules on the external surface of the graphene oxide may lead to crystal growth and the formation of a solid dispersion with crystals mixed with the amorphous form enwrapped in the graphene nanosheets. Nevertheless, the crystallinity of the loaded drug was reduced compared with the counterpart untreated drugs.

Fig. 7 shows a comparison of the adsorption and desorption of water vapor on 25% IBU/GO and the X-ray amorphous IBU. It was noticed that the moisture adsorption of the X-ray amorphous IBU was low, and the maximum amount of adsorption was about 0.15 wt%. Furthermore, there was a sudden drop in the amount of moisture adsorption at a P/P_0 of 60 to 70%, implying a physical transformation occurred at this stage. It is suggested that re-crystallization occurred when the X-ray amorphous IBU was exposed to moisture at a RH of 60–70% [30]. The physical transformation was not reversible; thus, the desorption profile was much lower, and a hysteresis loop at a P/P_0 of 10–70% was observed. In comparison, the X-ray amorphous form of IBU loaded on the graphene oxide showed different adsorption-desorption isotherms. The amount of moisture absorbed on IBU/GO increased with the increment in the P/P_0. The adsorption and desorption isotherms are almost identical without the presence of a hysteresis loop. The result implies that the X-ray amorphous form of IBU loaded on the graphene oxide was stable during the moisture adsorption test and that recrystallization of IBU was inhibited.

Fig. 8 shows a comparison of the dissolution profiles of FEN loaded on graphene oxide and untreated pure FEN crystal. The untreated FEN had a very low dissolution rate. In the first 20 min, only 6.9% of the FEN was dissolved and achieved 28% dissolution in 120 min. However, it was found that the dissolution rate of the FEN loaded on the graphene oxide was significantly enhanced. For three different loadings of FEN, the dissolution of FEN was more than 70% in 20 min., and it achieved above 88% dissolution in 60 min. The amorphous form of the FEN loaded on the graphene was believed to contribute to the rapid release. Although the sample with a high loading of 50 wt% FEN had some crystallinity revealed by the DSC and XRD, it may contain a mixture of amorphous and nano-crystalline FEN. The loaded amorphous part of FEN could contribute to the rapid initial burst release. The crystal part of the FEN resulted in a slightly slower dissolution compared to the pure amorphous formulation at the lower FEN loadings in the first 30 min. It was observed that the loaded drug reached a plateau level after 60 min and could not achieve 100% release in 2 h. The loaded FEN might not be fully released because some of the FEN was strongly adsorbed on the surface of the graphene oxide. Nevertheless, the percentage of this strongly adsorbed FEN was less than 10% because the specific surface area of graphene oxide is not as large as activated carbon. Fig. 9 shows the dissolution profiles of the 25 wt% IBU loaded on graphene oxide and the activated carbon. The untreated IBU crystal showed a low dissolution rate with only 11% dissolving in first 20 min. In comparison, 65% of the IBU loaded on the graphene oxide dissolved in the first 20 min. and achieved 82% dissolution in 2 h. It was observed that although the IBU loaded on activated carbon was also in X-ray amorphous form, only about 30% dissolution was achieved in the first 10 min, and there was no further substantial increment in the remaining 2 h dissolution test. Only 34% of the IBU was released from the IBU/AC sample in the 2 h of dissolution test. This result may indicate that a

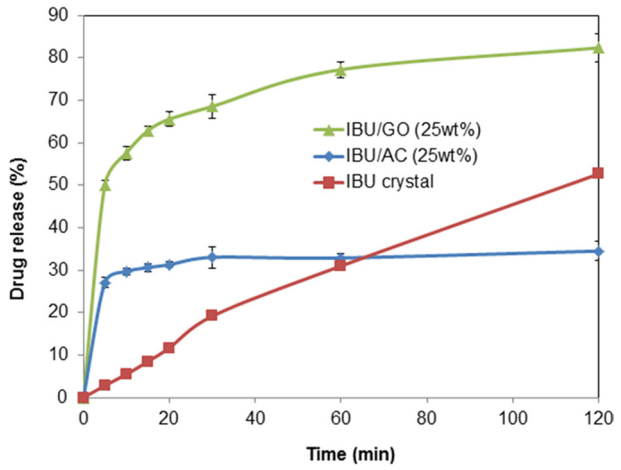

Fig. 9. Dissolution profiles of the IBU/GO, IBU/AC and compared with the untreated IBU crystal.

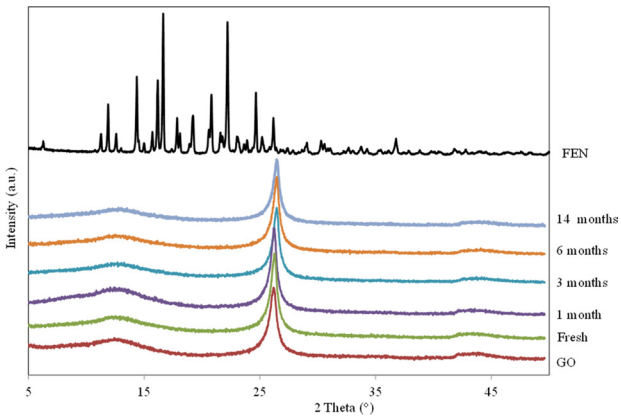

Fig. 10. XRD patterns of the 25 wt% FEN/GO after the storage test for different durations.

large portion of the IBU was retained in the porous structures of the AC. Due to the very large specific surface area, activated carbon is an excellent adsorbent for organic compounds [31,32]. The strong adsorption of IBU into the micro-porous structures limited the drug release, and only about 30% of the IBU located on the external surface or in larger pore channels could be released. In comparison, graphene oxide possesses the appropriate surface area for the X-ray amorphous IBU formulation and also had less retention of IBU on its surface. More than 80% of the IBU was released from the IBU/GO in 2 h and achieved a higher dissolution rate compared to the untreated IBU.

To increase the dissolution rate for poor water-soluble drugs, the formulation of APIs in amorphous form may be an effective approach. However, the stability of the amorphous form is a challenge because re-crystallization could occur during storage and transportation [33]. Fig. 10 shows the XRD patterns of co-spray-dried FEN and graphene oxide after the storage test under a stressed condition of 40°C and 75% RH for different periods. The enhanced dissolution rate of the graphene oxide loaded FEN is mainly attributed to the amorphous state of the FEN enwrapped in the graphene nanosheets; thus, its stability during storage is also one of the crucial factors to evaluate its potential for clinical applications. It was observed that the amorphous form of the FEN loaded on graphene oxide had excellent stability against re-crystallization during the accelerated storage test at 40°C and 75% RH. As shown in Fig. 10, graphene oxide had a characteristic X-ray diffraction peak at 2-theta of 26°. After loading with 25 wt% FEN, the diffraction pattern did not change, and no X-ray diffraction peaks assigned to crystalline FEN could be observed, reflecting the amorphous characteristics of the loaded FEN. It was found that the amorphous FEN enwrapped in the nanosheets of the graphene oxide had excellent stability during the accelerated storage test. After the storage test for 1, 3, 6 and 14 mo, no characteristic peaks for the FEN crystal could be detected by X-ray diffraction. Therefore, the graphene oxide loaded FEN interstices among the nanosheets in amorphous form due to the confined space, and the carbon nanosheets could effectively separate the amorphous particles of FEN to prevent re-crystallization and crystal growth under a high humidity condition. Because graphene is a strong and stable two dimensional nanomaterial, the movement of small API particles is limited. Thus, the formation of nuclei and the growth of crystal particles were inhibited once the API was enwrapped in the amorphous form. This formulation is different from other amorphous formations prepared with polymers to enhance the solubility. It was reported that the amorphous form can be achieved by formulation with polymers; however, recrystallization occurred during the storage test due to the low surface area and glass transition of polymer materials [34-36]. In this study, graphene oxide exhibited excellent properties as a drug carrier for the formulation of poorly soluble drugs in stable amorphous form with a significantly enhanced dissolution rate.

4. Conclusions

Graphene oxide was used as a drug carrier to formulate poorly water-soluble drugs by co-spray drying. The drugs enwrapped in "crumpled nanosheets" of graphene oxide were in X-ray amorphous form and exhibited a significantly enhanced dissolution rate compared with the untreated raw crystal drug. Although activated carbon has a high specific surface area and could also formulate poorly soluble drugs in an X-ray amorphous solid dispersion, the total drug release was limited to about 30% due to the microporous structure and large surface area of the activated carbon which strongly adsorbed the drug molecules and prevented their release to the aqueous based medium. In comparison, the nanosheets of the graphene had an adequate surface area and enwrapped the poorly water-soluble APIs in X-ray amorphous form which enabled the rapid release of more than 80% of the loaded drug. The nano-enwrapped amorphous formulations exhibited excellent stability during the storage test under stressed conditions for more than one year.

Conflict of Interest

No potential conflict of interest relevant to this article was reported.

Acknowledgements

Financial support for this study was provided by the Institute of Chemical and Engineering Sciences (ICES) under the Agency for Science, Technology and Research (A*STAR).

References

[1] Toda K, Furue, R, Hayami S. Recent progress in applications of graphene oxide for gas sensing: a review. Anal Chim Acta, **878**, 43 (2015). https://doi.org/10.1016/j.aca.2015.02.002.

[2] Chabot V, Higgins D, Yu AP, Xiao XC, Chen ZW, Zhang JJ. A review of graphene and graphene oxide sponge: material synthesis and applications to energy and the environment. Energy Environ Sci, **7**, 1564 (2014). https://doi.org/10.1039/c3ee43385d.

[3] OuYang FP, Huang B, Li ZY, Xiao J, Wang HY, Xu H. Chemical functionalization of graphene nanoribbons by carboxyl groups on Stone-Wales defects. J Phys Chem C, **112**, 12003 (2008). https://doi.org/10.1021/jp710547x.

[4] Zhu SM, Li JB, Chen YH, Chen ZX, Chen CX, Li Y, Cui ZW, Zhang D. Grafting of graphene oxide with stimuli-responsive polymers by using ATRP for drug release. J Nanopart Res, **14**, 1132 (2012). https://doi.org/10.1007/s11051-012-1132-x.

[5] Wang XM, Zhang WH. Application of graphene derivatives in cancer therapy: a review. New Carbon Mater, **28**, 321 (2013).

[6] Liu JG, Cui L, Losic D. Graphene and graphene oxide as new nanocarriers for drug delivery applications. Acta Biomater, **9**, 9243 (2013). https://doi.org/10.1016/j.actbio.2013.08.016.

[7] Yang K, Feng LZ, Liu Z. The advancing uses of nano-graphene in drug delivery. Expert Opin Drug Delivery, **12**, 601 (2014). https://doi.org/10.1517/17425247.2015.978760.

[8] Mianehrow H, Moghadam MHM, Sharif F, Mazinani S. Graphene-oxide stabilization in electrolyte solutions using hydroxyethyl cellulose for drug delivery application. Int J Pharm, **484**, 276 (2015). https://doi.org/10.1016/j.ijpharm.2015.02.069.

[9] Hou L, Shi YY, Jiang GX, Liu W, Han HL, Feng QH, Ren JX, Yuan YJ, Wang YC, Shi JJ, Zhang ZZ. Smart nanocomposite hydrogels based on azo crosslinked graphene oxide for oral colon-specific drug delivery. Nanotech, **27**, 315105 (2016). https://doi.org/10.1088/0957-4484/27/31/315105.

[10] Mianehrow H, Afshari R, Mazinani S, Sharif F, Abdouss M. Introducing a highly dispersed reduced graphene oxide nano-biohybrid employing chitosan/hydroxyethyl cellulose for controlled drug delivery. Int J Pharm, **509**, 400 (2016). https://doi.org/10.1016/j.ijpharm.2016.06.015.

[11] Wang WN, He X. Aerosol processing of crumpled graphene oxide-based nanocomposites for drug delivery. Curr Pharm Des, **22**, 2491 (2016). https://doi.org/10.2174/1381612822666160128145456.

[12] Ma NX, Zhang BH, Liu J, Zhang P, Li ZB, Luan YX. Green fabricated reduced graphene oxide: evaluation of its application as nano-carrier for pH-sensitive drug delivery. Int J Pharm, **496**, 984 (2015). https://doi.org/10.1016/j.ijpharm.2015.10.081.

[13] Zheng XT, Ma XQ, Li CM. Highly efficient nuclear delivery of anti-cancer drugs using a bio-functionalized reduced graphene oxide. J Colloid Interface Sci, **467**, 35 (2016). https://doi.org/10.1016/j.jcis.2015.12.052.

[14] Wei YC, Zhou FF, Zhang, Chen Q, Xing D. A graphene oxide based smart drug delivery system for tumor mitochondria-targeting photodynamic therapy. Nanoscale, **8**, 3530 (2016). https://doi.org/10.1039/c5nr07785k.

[15] Tian JW, Luo YP, Huang LW, Feng YQ, Ju HX, Yu BY. Pegylated folate and peptide-decorated graphene oxide nanovehicle for in vivo targeted delivery of anticancer drugs and therapeutic self-monitoring. Biosens Bioelectron, **80**, 519 (2016). https://doi.org/10.1016/j.bios.2016.02.018.

[16] Wang GS, Ma YY, Wei ZY, Qi M. Development of multifunctional cobalt ferrite/graphene oxide nanocomposites for magnetic resonance imaging and controlled drug delivery. Chem Eng J, **289**, 150 (2015). https://doi.org/10.1016/j.cej.2015.12.072.

[17] Yang Y, Shi HL, Wang YP, Shi BZ, Guo LL, Wu DM, Yang SP, Wu HX. Graphene oxide/manganese ferrite nanohybrids for magnetic resonance imaging, photothermal therapy and drug delivery. J Biomater Appl, **30**, 810 (2016). https://doi.org/10.1177/0885328215601926.

[18] Justin R, Tao K, Román S, Chen DX, Xu YW, Geng XS, Ross IM, Grant RT, Pearson A, Zhou GD, MacNeil S, Sun K, Chen BQ. Photoluminescent and superparamagnetic reduced graphene oxide–iron oxide quantum dots for dual-modality imaging, drug delivery and photothermal therapy. Carbon, **97**, 54 (2016). https://doi.org/10.1016/j.carbon.2015.06.070.

[19] Li B, Yang J, Huang Q, Zhang Y, Peng C, Zhang Y, He Y, Shi JY, Li WX, Hu J, Fan CH. Biodistribution and pulmonary toxicity of intratracheally instilled graphene oxide in mice. NPG Asia Mater, **5**, e44 (2013). https://doi.org/10.1038/am.2013.7.

[20] Schinwald A, Murphy F, Askounis A, Koutsos V, Sefiane K, Donaldson K, Campbell CJ. Minimal oxidation and inflammogenicity of pristine graphene with residence in the lung. Nanotoxicology, **8**, 824 (2013). https://doi.org/10.3109/17435390.2013.831502.

[21] Schinwald A, Murphy FA, Jones A, Macnee W, Donaldson K. Graphene-based nanoplatelets: a new risk to the respiratory system as a consequence of their unusual aerodynamic properties. ACS Nano, **6**, 736 (2012). https://doi.org/10.1021/nn204229f.

[22] Yang K, Gong H, Shi X, Wan J, Zhang Y, Liu Z. In vivo biodistribution and toxicology of functionalized nano-graphene oxide in mice after oral and intraperitoneal administration. Biomaterials, **34**, 2787 (2013). https://doi.org/10.1016/j.biomaterials.2013.01.001.

[23] Fu C, Liu T, Li L, Liu H, Liang Q, Meng X. Effects of graphene oxide on the development of offspring mice in lactation period. Biomaterials, **40**, 23 (2015). https://doi.org/10.1016/j.biomaterials.2014.11.014.

[24] Santos H, Peltonen L, Limnell T, Hirvonen J. Mesoporous materials and nanocrystals for enhancing the dissolution behavior of poorly water-soluble drugs. Curr Pharm Biotechnol, **14**, 926 (2013). https://doi.org/10.2174/13892010146661312261504O4.

[25] Vialpando M, Martens, JA, Van den Mooter G. Potential of ordered mesoporous silica for oral delivery of poorly soluble drugs. Ther Delivery, **2**, 1079 (2011). https://doi.org/10.4155/tde.11.66.

[26] Shen SC, Ng WK, Chia LO, Dong YC, Tan RH. Applications of mesoporous materials as excipients for innovative drug delivery and formulation. Curr Pharm Des, **19**, 6270 (2013). https://doi.org/10.2174/1381612811319350005.

[27] Zhao P, Wang LH, Sun CS, Jiang TY, Zhang JH, Zhang Q, Sun J, Deng YH, Wang SL. Uniform mesoporous carbon as a carrier for poorly water soluble drug and its cytotoxicity study. Eur J Pharm Biopharm, **80**, 535 (2012). https://doi.org/10.1016/j.ejpb.2011.12.002.

[28] McCarthy CA, Ahern RJ, Dontireddy R, Ryan KB, Crean AM. Mesoporous silica formulation strategies for drug dissolution enhancement: a review. Expert Opin Drug Delivery, **13**, 93 (2016). https://doi.org/10.1517/17425247.2016.1100165.

[29] Hong SQ, Shen SC, Tan DCT, Ng WK, Liu XM, Chia LSO, Irwan AW, Tan R, Nowak SA, Marsh K, Gokhale R. High drug load, stable, manufacturable and bioavailable fenofibrate formulations in mesoporous silica: a comparison of spray drying versus solvent impregnation methods. Drug Delivery, **23**, 316 (2016). https://doi.org/10.3109/10717544.2014.913323.

[30] Lim RTY, Ng WK, Widjaja E, Tan RBH. Comparison of the physical stability and physicochemical properties of amorphous indomethacin prepared by co-milling and supercritical anti-solvent co-precipitation. J Supercritical Fluids, **79**, 186 (2013). https://doi.org/10.1016/j.supflu.2013.02.017.

[31] Mestre AS, Pires RA, Aroso I, Fernandes EM, Pinto ML, Reis RL, Andrade MA, Pires J, Silva SP, Carvalho AP. Activated carbons prepared from industrial pre-treated cork: Sustainable adsorbents for pharmaceutical compounds removal. Chem Eng J, **253**, 408 (2014). https://doi.org/10.1016/j.cej.2014.05.051.

[32] Bhadra BN, Ahmed I, Kim S, Jhung SH. Adsorptive removal of ibuprofen and diclofenac from water using metal-organic framework-derived porous carbon. Chem Eng J, **314**, 50 (2017). https://doi.org/10.1016/j.cej.2016.12.127.

[33] Wu Q, Kennedy MT, Nagapudi K, Kiang YH. Humidity induced phase transformation of poloxamer 188 and its effect on physical stability of amorphous solid dispersion of AMG 579, a PDE10A inhibitor. Int J Pharm, **521**, 1 (2017). https://doi.org/10.1016/j.ijpharm.2017.01.059.

[34] Marsac PJ, Konno H, Rumondor ACF, Taylor LS. Recrystallization of nifedipine and felodipine from amorphous molecular level solid dispersions containing poly(vinylpyrrolidone) and sorbed water. Pharm Res, **25**, 647 (2008). https://doi.org/10.1007/s11095-007-9420-3.

[35] Martínez-Ohárriz MC, Rodríguez-Espinosa C, Martín C, Goñi MM, Tros-Ilarduya MC, Sánchez M. Solid dispersions of diflunisal–PVP: polymorphic and amorphous states of the drug. Drug Dev Ind Pharm, **28**, 717 (2002). https://doi.org/10.1081/ddc-120003864.

[36] Lim RTY, Ng WK, Tan RBH, Dissolution enhancement of indomethacin via amorphization using co-milling and supercritical co-precipitation processing. Powder Technol, **240**, 79 (2013). https://doi.org/10.1016/j.powtec.2012.07.004.